# CALIBRATION AND TESTING OF SALINE SOIL PARAMETERS BASED ON EDEM DISCRETE ELEMENT METHODOLOGY

/

# 基于 EDEM 离散元方法的盐碱土壤参数标定与测试

**Xiaoning HE[1)], Shikuan MA[1)], Zhixin LIU[1)], Dongwei WANG[1)], Shuqi SHANG [*1)], Guanghui LI[2)], Hongxiu LI[2)]**

[1)] College of Electrical and Mechanical Engineering, Qingdao Agricultural University, Qingdao/ China [1)]

[2)] Shandong Saline Modern Agriculture Co., Ltd, Dongying / China [2)]

*Corresponding author: Shuqi SHANG*

*Tel: +8618306391208; E-mail: 944286200@qq.com*

*DOI: https://doi.org/10.35633/inmateh-73-69*

***Keywords:*** *EDEM; saline soil; Parameter calibration*

**ABSTRACT**

*In this study, saline soil parameters were calibrated based on EDEM discrete element method, soil density, soil elastic modulus, soil shear modulus, soil particle size distribution and Poisson's ratio were determined. The Hertz-Mindlin with Johnson-Kendall-Roberts (JKR) model was used to simulate the characteristics of soil stress and strain of particles under external forces. The JKR contact parameter between saline soil particles was used as a test factor, and the soil accumulation angle was used as a test index to carry out the saline soil contact parameter calibration test. It was finally determined that an elastic recovery coefficient of 0.262, a static friction coefficient of 0.263, a dynamic friction coefficient of 0.234, and a JRK surface energy of 10.084 were the optimal combinations of contact parameters for saline soils.*

**摘要**

*本研究基于 EDEM 离散元法对盐碱土壤参数参数进行标定，通过测定土壤密度、土壤弹性模量、土壤剪切模量、土壤粒径分布及泊松比。采用 Hertz-Mindlin with Johnson-Kendall-Roberts 模型模拟颗粒在外力作用下的土壤应力与应变的特征。将盐碱土壤颗粒间的 Hertz-Mindlin with Johnson-Kendall-Roberts 接触参数作为试验因素，以土壤堆积角作为试验指标，进行盐碱土壤接触参数标定试验。最终确定弹性恢复系数 0.262、静摩擦系数 0.263、动摩擦系数 0.234、JRK 表面能 10.084 是盐碱土壤的最优接触参数组合。*

## INTRODUCTION

Studies have shown that analysing the interaction between saline soils and agricultural machinery is essential for developing agricultural machinery and equipment suitable for such lands *(Xing et al., 2020; Xu et al., 2005; Abo-Elnor M. et al., 2004)*. The discrete element method can be used to simulate and analyse the interactions between agricultural bulk materials and machinery and equipment, which saves time and effort and provides more accurate data for the design of agricultural machinery and equipment due to its high visibility and accuracy compared to traditional field tests *(Chen et al., 2021; Zeng et al., Yu et al., 2005; Tong J et al., 2010)*. In order to effectively predict the soil rheology under the interactions with touching soil components, parameter calibration and discrete element modelling of different types of soils are required, which have been studied by scholars at home and abroad. *Song et al. (2022)* and *Han et al. (2021)* determined the particle mechanics parameters of mulberry orchard soil and Xinjiang orchard deep applied bulk respectively, which can be used for the discrete element simulation analysis of the interaction between soil touching parts and soil of mulberry orchard tillage machinery in sandy loam soil and its structural optimization. *Aikins et al. (2021),* calibrated the contact parameters of Hysteretic Spring model and Linear Cohesion model for cohesive soil and verified their accuracy through the performance test of trencher. *Qiu Y. et al. (2022),* took brown soil as the research object and calibrated the relevant model parameters of brown soil by using EDEM simulation software, which provided basic data for the simulation study of cutting resistance of brown soil touching parts.

---

[1] *Xiaoning HE, Prof. Ph.D. Eng.; Shikuan MA, M.S. Stud. Eng.; Zhixin LIU, M.S. Stud. Eng.; Dongwei WANG, Prof. Ph.D. Eng.; Shuqi SHANG, Prof. Ph.D. Eng.*

[2] *Guanghui LI, M.S. Stud. Eng.; Hongxiu LI, M.S. Stud.*

*Luo et al., (2018),* proposed a method for the determination of the angle of repose of the bulk, through the JKR bonding model between the particles to reflect the matrix viscosity, and established a mapping relationship with the angle of repose. *Zhang et al., (2023)* characterised the nature of the discrete elements of the soil in terms of several parameters by carrying out a stacking test with the angle of repose as the target. *Tian et al., (2021),* used the Plackett- Burman test, the steepest climb test and so on to screen out the optimal range of values of the salient parameters, and then take the actual stacking angle as the target, and use the software optimisation function to optimise the salient parameters and get the optimal parameter combinations. *Wang et al., (2017),* and *Hao et al., (2023),* used the particle rheology parameter model for tyre compaction interaction simulation and rotary ploughing test to verify the validity of the calibrated results. *Wang X. et al., (2019),* investigated the effect of different modelling particle radii on the interaction process by establishing a soil-plough interaction model, and obtained the optimal value of the particle radius of the soil model through the index of crushing and traction force and other indexes. *Li J.W. et al., (2019),* calibrated the parameters of two kinds of clayey black soils with different water content in Northeast China, and provided simulation parameters for the design and optimisation of bionic drag reduction of touching parts of agricultural machinery under the operating conditions of clayey black soils in Northeast China.

Therefore, according to the characteristics of saline soil in Dongying City, based on the soil accumulation test, combined with experimental measurements, this study uses EDEM software to construct a soil simulation model, takes the accumulation angle as the evaluation index, and employs Design Expert software to determine the optimal values of soil simulation parameters, and carries out the calibration test of saline soil contact parameters, so as to provide the necessary discrete element simulation for the further research on the interaction between saline soil and soil touching components, basic parameters required for discrete element simulation.

## MATERIAL AND METHODS

### *Particle modelling of saline soils*

Five 100×100 cm sampling blocks were selected by five-point sampling method, as shown in Fig. 1. Soil particle size distribution determination, soil stacking angle determination and soil hardsetting determination were carried out at the sampling site for soil density determination, soil elastic modulus determination and soil shear modulus determination, respectively.

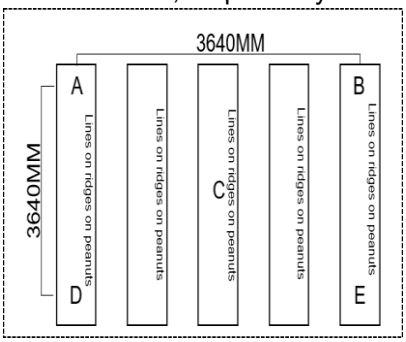


**Fig. 1 – Field soil sampling**

### *Density determination of saline soils*

The cylinder method is chosen to determine the density of saline soils, the principle of the cylinder method is the ratio of the mass of the soil in the cylinder to the internal volume of the cylinder, the mass of the soil inside the cylinder can be weighed first after the mass of the cylinder and the soil and then subtracted from the mass of the cylinder itself, the formula for the calculation is:

$$\rho = \frac{m_1 - m_2}{V} \times 100\% \quad (1)$$

where:

$\rho$ is the soil density, [%]; $m_1$ is the total mass of soil sample and ring cutter, [kg]; $m_2$ is the clean cylinder quality, [kg]; $V$ is the ring cutter volume, [cm$^3$].

Sampling in order to avoid different depths of the soil density is different, the depth of sampling will be divided into three levels, respectively, 0-5, 5-10, 10-15 cm. The same randomly take five samples in each layer, the average value, which can be obtained from the density of the soil layer, will be selected for five sampling. The five selected sampling blocks, are in accordance with the above steps for soil density determination test, the density data of different soil layers of each sampling block are shown in Fig. 2.

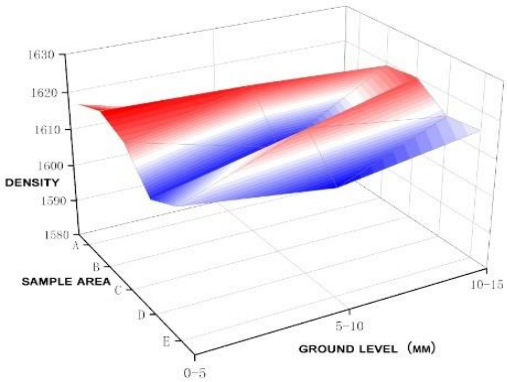


**Fig. 2 – Soil Density by Survey Area**

According to the data in Fig. 2, it can be seen that the location and depth 0-15 cm of saline soil have less effect on its soil density, so the soil density is taken as 1622.5 kg/m$^3$.

***Determination of shear modulus of saline soils***

Soil shear modulus can be determined by straight shear test, the principle of soil direct shear test is based on Coulomb's law, given a vertical stress on the test soil sample, to determine the maximum shear force that can be withstood laterally by the test soil sample under the action of the vertical stress, so as to find out the coefficient of kinetic friction between saline and alkaline soils (*Xiang et al, 2019)*.

This test is a fast shear test, using ZJ strain-controlled direct shear apparatus (referred to as direct shear apparatus in this paper). The test steps are as follows: four soil samples (soil samples) of saline-alkali soil were prepared by the ring knife of the direct shear apparatus in each sample area, and the ZJ strain-controlled direct shear apparatus was adjusted. As shown in Fig. 3, the water stone and the absorbent paper were placed in the interior of the shear box, and the ring knife with the soil sample was placed on the shear plate, and then the absorbent paper, the water stone and the shear box cover were placed in turn. The soil was pressed into the shear box with the box cover, and the pressure device was installed after the ring knife was removed, put the screws on the box cover and tighten the screws with a little force, rotate the handwheel clockwise, adjust the measuring force ring, set the percentage meter to zero, put the cover plate and the ball pressure frame in turn, and add weights to each group of soil specimens so that the vertical stress is 100 kPa, 200 kPa, 300 kPa, 400 kPa. Turn on the switch of the straight shear instrument so that the soil specimen is sheared in 3-5 minutes, and record the value of the gauge once every 1 s. Record the value of the recording gauge repeat the test 5 times and take the average value *(Zhang et al, 2022)*.

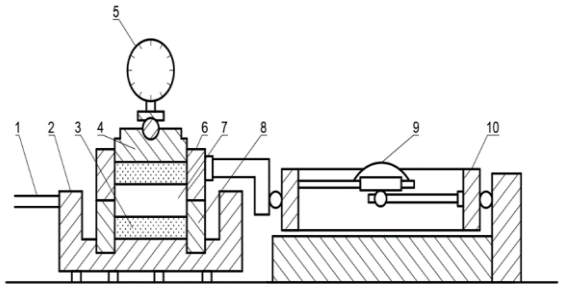


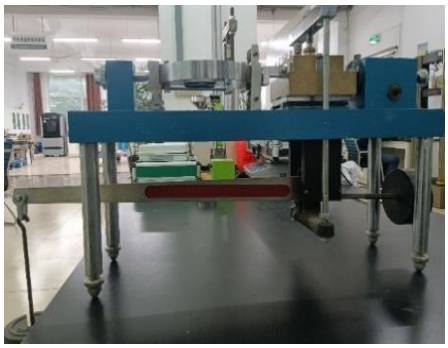

**Fig. 3 – ZJ type strain control type straight shear instrument**

*1. axle; 2. base; 3. permeable stone; 4. piston; 5. gauge; 6. upper box; 7. soil sample; 8. lower box; 9. gauge; 10. gauge ring*

The shear strength and the shearing displacement is given as:

$$\tau_0 = CR,\ \Delta L = tv \tag{2}$$

where:

$\tau_0$ is the shear strength, [kPa]; *C* is the proving ring correction coefficient unit, 1.506; $R$ is the proving ring readings, 0.01 mm; $\Delta L$ is the shear displacement, [mm]; *t* is the times, [s]; $v$ is the shear rate, 0.08 mm/min.

Taking $\tau_0$ as the vertical coordinate and $\Delta L$ as the horizontal coordinate, the relationship curve is obtained, as shown in Fig. 4.

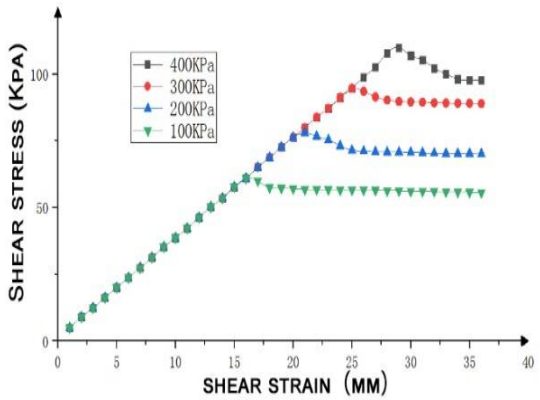


**Fig. 4 – Shear Displacement-Shear Stress Relationship Curve**

The magnitude of the measured soil shear strength is shown in Table 1. The shear modulus of saline soil is $3.76\times10^7$ Pa, it can be calculated from the shear displacement-shear stress relationship curve with Table 1:

$$G = \frac{\tau_0}{\Delta L} \tag{3}$$

**Table 1**

**Shear strength magnitudes**

| Vertical pressure (kPa) | 100 | 200 | 300 | 400 |
|---|---|---|---|---|
| Maximum deformation of measuring ring: $R$（0.01 mm） | 33 | 48.5 | 68.5 | 91.5 |
| Shear strength | 49.698 | 73.04 | 103.16 | 137.80 |
| Quantitative force loop coefficient: $C$（kPa/0.01 mm） | 1.506 | | | |
| Gauge Ring Number | 07439 | | | |

***Particle size distribution and Poisson's ratio of saline soil***

The percentage of soil particle size distribution is the distribution ratio of soil particles in the field, and the soil texture can also be determined by the percentage of soil particle size distribution. The main steps of the soil particle size distribution percentage determination test are as follows: first, a certain number of soil samples needs to be taken and completely dried. The purpose of drying is to remove water from the soil in order to more accurately measure the particle size distribution of soil particles. Then, the JA21002 electronic precision balance (0.01 g) produced by Shanghai Jingtian Electronic Instrument Co., Ltd. was used to weigh and record the total mass of the sample. Finally, a series of standard sieves were used for screening, and the soil analysis sieve produced by Nanjing Soil Instrument Factory Co., Ltd. was used for screening. The apertures of each sieve were 2.0 mm, 1.0 mm, and 0.5 mm, respectively, fully vibrated for 20 minutes, and then the soil quality of each sieve surface was weighed by JA21002 electronic precision balance (*He et al, 2021*). The proportion of soil mass of each sieve to the total mass of the sample is calculated, which is the percentage of soil particle size distribution.

The calculation formula is:

$$x = \frac{m_i}{m_A} \times 100\% \tag{4}$$

where: $x$ is the percentage by mass of soil particles of a given size, [%]; $m_i$ is the mass of soil particles of a given size, [kg]; $m_A$ is the total mass of soil sample, [kg].

Firstly, the soil pretreatment was carried out, and the collected soil was placed in a ventilated and dry room to air-dry for a period of time, and then the dried soil was crushed and passed through a standard sieve with a pore size of 2 mm, and stored in a container for spare.

Then the specific gravity meter method was used to determine the particle size distribution of the collected saline soil, the soil particle size percentage test was repeated five times for each sampling block, the average value of the soil particle size distribution percentage was calculated. After statistical analysis, the particle size distribution of saline soil in each sampling block is shown in Figure 5.

**Table 2**

**Name of soil particle composition and texture**

| | Particle content / % | | | Soil condition |
|---|---|---|---|---|
| sampling area | ＜0.002 mm (clay content) | 0.02～0.002 mm (silt content) | ＞0.02 mm (sand content) | |
| A | 12.7 | 30.6 | 56.7 | |
| B | 11.8 | 32.1 | 56.1 | sandy loam |
| C | 13.6 | 29.5 | 56.9 | |
| D | 12.2 | 31.9 | 55.9 | |
| E | 13.1 | 29.8 | 57.1 | |

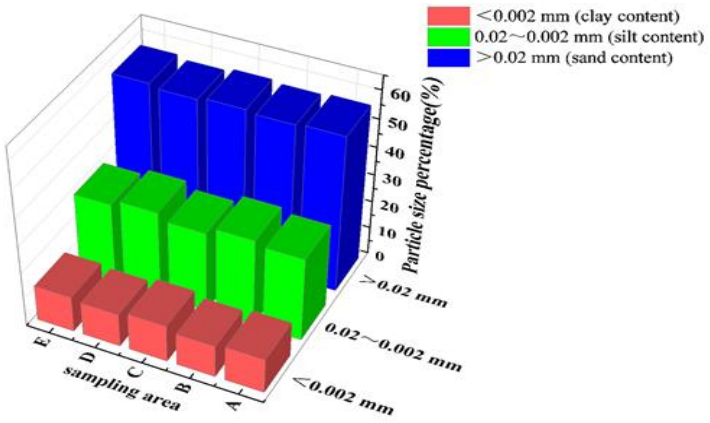


**Fig. 5 – Saline soil particle size distribution**

As can be seen from Figure 5, the saline soil grain size is mainly distributed in the >2 mm sandy loam interval, and the saline soil type can be obtained as chalky clay according to the International Soil Classification Standard.

The modulus of elasticity of soil is the instantaneous stress-strain modulus under un-lateralised conditions, and soil is not an ideal elastomer. A microcellular body taken from a laterally impermissible expansion compression soil sample was analysed under pressure in the Z-axis direction and was subjected to a positive stress of $\sigma_Z$ , and its positive stress in the horizontal direction was:

$$\sigma_x = \sigma_y = K_0\sigma_Z \tag{5}$$

Where:

$K_0$ is the coefficient of earth pressure at rest.

Analysing strain in the x-direction:

$$\varepsilon_x = \frac{\sigma_x}{E_0} - \mu\frac{\sigma_y}{E_0} - \mu\frac{\sigma_2}{E_0} = 0 \tag{6}$$

The relationship between soil pressure coefficient and Poisson's ratio can be obtained by joining the two equations:

$$\mu = \frac{K_0}{(1+K_0)} \tag{7}$$

According to the type and state of the soil, the empirical value can be selected. The saline-alkali soil is silty clay, check 'mechanical soil dynamics' and 'soil mechanics', $K_0$ is 0.43, and the Poisson's ratio of the saline-alkali soil is 0.30.

***Generate EDM particles***

In conjunction with the determination of the soil intrinsic parameters, the saline soil intrinsic parameters were: density 1622.5 kg/m$^3$, Poisson's ratio 0.30, shear modulus 3.76×107 Pa. Simplified setting of the particle size and mass percentage of the soil were: 27% for 1 mm; 48.4% for 1.5 mm; and 24.6% for 2.0 mm.

***Determination of particle contact models for saline soils***

The JKR model can be used to simulate the characteristics of soil stress and strain of particles under external forces, which not only reflects the elasticity and plasticity of the particles, but also the bonding of the particles, which is shown schematically in Fig. 6.

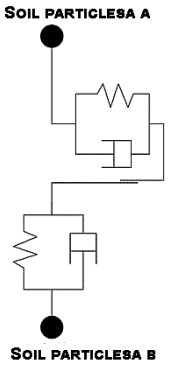


**Fig. 6 – Schematic of soil particle contact modeling**

To represent the cohesive force between particles, the normal elastic contact force of the JKR model is shown in Formula (8). The equivalent elastic modulus can be expressed by Formula (9). The equivalent contact radius is shown in Formula (10). The tangential overlap and normal overlap satisfy Formula (11).

$$F_{JKR} = -4\sqrt{\pi\gamma E^*}a^{\frac{3}{2}} + \frac{4E^*}{3R^*}a^3 \quad (8)$$

$$\frac{1}{E^*} = \frac{1-v_1^2}{E_1^*} + \frac{1-v_2^2}{E_2^*} \quad (9)$$

$$\frac{1}{R^*} = \frac{1}{R_1} + \frac{1}{R_2} \quad (10)$$

$$\delta = \frac{a^2}{R^*} - \sqrt{\frac{4\pi\gamma a}{E^*}} \quad (11)$$

where:

$F_{JKR}$ is the JKR normal contact elastic force; $E^*$ is the equivalent elastic modulus, [Pa]; $R^*$ is the equivalent contact radius, [m]; $a$ is the tangential overlap amount, [m]; $\gamma$ is the surface tension, [N/m]; $E_1^*$ is the elastic modulus of particle 1, [Pa]; $E_2^*$ is the elastic modulus of particle 2; $v_1$ is the Poisson 's ratio of particle 1; $v_2$ is the Poisson 's ratio of particle 2; $R_1$ is the contact radius of particle 1, [m]; $R_2$ is the contact radius of particle 2, [m].

If there is no contact between the particles, the particles have a cohesive force that attracts each other. The maximum gap between the particles with non-zero cohesion is calculated according to Formula (12).

$$\delta_c^* = \frac{a_c^2}{R^*} - \sqrt{\frac{4\pi\gamma a_c}{E^*}} \quad a_c = \frac{9\pi\gamma R^{*2}}{2E^*}\left(\frac{3}{4} - \frac{1}{\sqrt{2}}\right) \quad (12)$$

where:

$\delta_c$ is the maximum normal gap when there is non-zero cohesion between particles, [m]; $a_c$ is the maximum tangential gap when there is non-zero cohesion between particles, [m].

The saline-alkali soil has the characteristics of compaction and stratification. The Hertz-Mindlin with bonding contact model is selected for the saline-alkali compaction layer. As shown in Fig. 7, in this paper, the soil particle radius is set to 1 mm, and the particle bond radius is 2 mm. The normal stiffness per unit area of the model is $3.5\times10^7$ N/m$^3$, the tangential stiffness per unit area is $2.4\times10^7$ N/m$^3$, the critical normal stress is $3.1\times10^7$ Pa, and the critical tangential stress is $2.1\times10^7$ Pa.

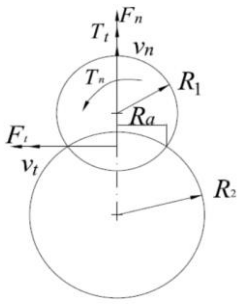


**Fig. 7 – Force diagram of bonded bond**

When the normal stress and tangential stress between soil particles reach a certain extreme value, the bonding bond between soil particles will break, assuming that the normal stress and tangential stress are $\sigma_{max}\tau_{max}$, $\tau_{max}$. According to Formula (13), when the bonding bond breaks, it satisfies Formula (14), so as to determine the critical normal stress and critical tangential stress at the time of fracture.

$$\begin{cases} \delta F_n = -v_n k_n A \delta_t \\ \delta F_t = -v_t k_t A \delta_t \\ \delta M_n = -w_n k_t A \delta_t \\ \delta M_t = -w_t k_t \frac{j}{2} \delta_t \\ A = \pi R_B \\ J = \frac{1}{2}\pi R_B^4 \end{cases} \quad (13)$$

$$\begin{cases} \sigma_{max} < \frac{-F_n}{A} + \frac{2M_t}{J} R_B \\ \tau_{max} < \frac{-F_t}{A} + \frac{M_n}{J} R_B \end{cases} \quad (14)$$

where: $F_n$ is the normal contact force, [N]; $F_t$ is the tangential contact force, [N]; $v_n$ is the normal velocity, [m/s]; $v_t$ is the tangential velocity, [m/s]; $k_n$ is the normal stiffness, [N/m]; $k_t$ is the tangential stiffness, [N/m]; $w_n$ is the normal angular velocity, [rad/s]; $w_t$ is the tangential angular velocity, [rad/s]; *A* is the unit contact area, [mm$^2$]; *J* - is the moment of inertia, [mm$^4$]; $M_t$ is the normal torque between particles, [N·m]; $M_n$ is the tangential torque between particles, [N·m]; $\delta_t$ is the time step, [s]; $R_B$ is the particle bond radius, [mm].

***Saline soil calibration test***

The JKR contact parameters (coefficient of elastic recovery, coefficient of static friction, coefficient of kinetic friction, and JRK surface energy) between the saline soil particles were used as the test factors, and the soil stacking angle was used as the test index for the saline soil contact parameter calibration test (*Wang et al, 2019*). The experimental principle is shown in Fig.8. The inclination measuring instrument is placed above the soil plate, and the inclination measuring instrument is adjusted to 0°. Then the funnel of organic glass is placed on the test frame, so that the saline-alkali soil falls naturally from the upper end of the funnel under the action of gravity. After the soil falls off, the soil accumulation angle is measured. The soil accumulation angle was measured four times for each of the five sampling blocks, recorded and statistically analysed as shown in Fig. 9, which gives an actual soil accumulation angle of 36.6° with a standard deviation of 0.45.

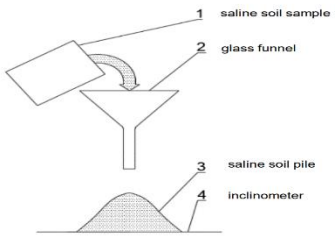


**Fig. 8 – Principle of determination of accumulation angle of saline soil**

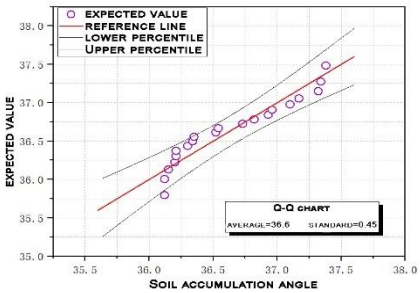


**Fig. 9 – Statistical Analysis of Soil Stockpile Angles**

Referring to the GEMM database in EDEM2021, the recommended range of values for the contact parameters was obtained based on the basic physical parameters of saline soils and the soil accumulation angle, with the factor codes as shown in Table 2, and the contact parameter calibration test was conducted for saline soils according to the four-factor quadratic orthogonal rotational combination test programme.

**Table 2**

**Factor Coding Table**

| Code | A | B | C | D |
|---|---|---|---|---|
| +2 | 0.40 | 0.30 | 0.45 | 14.5 |
| +1 | 0.33 | 0.238 | 0.363 | 11.75 |
| 0 | 0.26 | 0.175 | 0.275 | 9 |
| -1 | 0.19 | 0.113 | 0.188 | 6.25 |
| -2 | 0.12 | 0.05 | 0.10 | 3.5 |

***Simulation test of soil accumulation angle***

The simulation test of soil stacking angle was carried out in EDEM2021 at a ratio of 1:1. The other contact parameters in the simulation test were obtained by consulting the mechanical design manual, and the contact parameters between them can be obtained by referring to the relevant literature, and the simulation parameters are shown in Table 3.

**Table 3**

**Parameters related to soil stacking angle simulation test**

| analogue parameter | numerical value | analogue parameter | numerical value |
|---|---|---|---|
| Saline soil density | 1622.5$kg/m^3$ | Collision recovery coefficient between saline soil and -65Mn steel | 0.12 |
| Poisson's ratio for saline soils | 0.30 | Coefficient of static friction between saline soil-65Mn steel | 0.39 |
| Shear modulus of saline soils | $5.74\times10^6 Mpa$ | Sliding friction coefficient between saline soil-65Mn steel | 0.08 |
| 65Mn steel density | 7830$kg/m^3$ | Coefficient of recovery for collisions between saline soils and -glass | 0.15 |
| Poisson's ratio of 65Mn steel | 0.29 | Coefficient of static friction between saline soil-glass | 0.48 |
| 65Mn steel shear modulus | $7.9\times10^{10}$ | Coefficient of sliding friction between saline soil-glass | 0.11 |
| Glass density | 1190 | gravitational acceleration（$m/s^2$） | 9.8 |
| Glass Poisson's ratio | 0.29 | time step: $s$ | 1.20e-05 |
| Glass shear modulus | $1.28\times10^9$ | simulation duration: $s$ | 5 |

The simulation mimics the soil accumulation angle test, looking squarely at the X and Y axes and using the post-processing tool Protractor, the soil particles accumulation angle was measured, as shown in Fig. 10, and a total of four measurements were taken in each direction, and the average value was taken and recorded.

## RESULTS

***Simulation results***

The simulation model of soil repose angle is shown in Fig.10. Among them, the funnel-shaped diversion curved wall adopts smooth glass material, its Poisson 's ratio is 0.24, the density is 1190 kg/m$^3$, and the shear modulus is 1.28 × 109 Pa. The selection range of soil contact parameters is shown in Table 3. The aggregate groups of soil samples in each plough layer were established by EDEM particle element function. In the process of settlement, it stabilizes the downflow by gravity acceleration, squeezes and deforms between aggregates, and forms a stacking effect on the receiving plate. Then, according to the four-factor quadratic orthogonal rotation combination test design method, the test scheme is compiled for the data in table 2, and the simulation test of soil accumulation angle measurement is carried out according to the test scheme. In order to avoid the error in each calculation process, each test group will be repeated three times. The average value is used as the test result. After determining the test result, the difference between the test result and the actual soil accumulation angle is made. The test scheme and its result are shown in table 4.

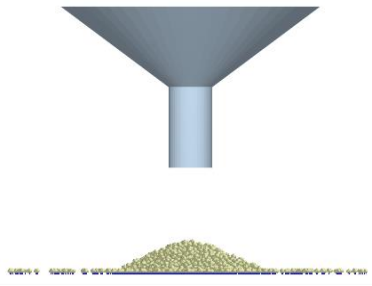

Fig. 10 – Soil accumulation angle simulation test

Table 4

Test Program and Results

| NO. | A | B | C | D | 1 |
|---|---|---|---|---|---|
| 1 | 0.19 | 0.1 | 0.15 | 6 | 2.73 |
| 2 | 0.33 | 0.1 | 0.15 | 6 | 2.59 |
| 3 | 0.19 | 0.2 | 0.15 | 6 | 2.5 |
| 4 | 0.33 | 0.2 | 0.15 | 6 | 2.44 |
| 5 | 0.19 | 0.1 | 0.25 | 6 | 3.27 |
| 6 | 0.33 | 0.1 | 0.25 | 6 | 2.91 |
| 7 | 0.19 | 0.2 | 0.25 | 6 | 2.79 |
| 8 | 0.33 | 0.2 | 0.25 | 6 | 2.38 |
| 9 | 0.19 | 0.1 | 0.15 | 12 | 2.29 |
| 10 | 0.33 | 0.1 | 0.15 | 12 | 2.64 |
| 11 | 0.19 | 0.2 | 0.15 | 12 | 2.49 |
| 12 | 0.33 | 0.2 | 0.15 | 12 | 2.66 |
| 13 | 0.19 | 0.1 | 0.25 | 12 | 2.68 |
| 14 | 0.33 | 0.1 | 0.25 | 12 | 2.65 |
| 15 | 0.19 | 0.2 | 0.25 | 12 | 2.58 |
| 16 | 0.33 | 0.2 | 0.25 | 12 | 2.46 |
| 17 | 0.12 | 0.15 | 0.2 | 9 | 2.76 |
| 18 | 0.4 | 0.15 | 0.2 | 9 | 2.56 |
| 19 | 0.26 | 0.05 | 0.2 | 9 | 2.54 |
| 20 | 0.26 | 0.25 | 0.2 | 9 | 2.16 |
| 21 | 0.26 | 0.15 | 0.1 | 9 | 2.41 |
| 22 | 0.26 | 0.15 | 0.3 | 9 | 2.81 |
| 23 | 0.26 | 0.15 | 0.2 | 3 | 2.95 |
| 24 | 0.26 | 0.15 | 0.2 | 15 | 2.75 |
| 25 | 0.26 | 0.15 | 0.2 | 9 | 2.65 |
| 26 | 0.26 | 0.15 | 0.2 | 9 | 2.62 |
| 27 | 0.26 | 0.15 | 0.2 | 9 | 2.64 |

***Analysis of test results***

In order to analyse the test factors that have a significant effect on the simulated stacking angle, the test results were analysed by ANOVA, as shown in Table 5.

Table 5

Analysis of Variance (ANOVA) for Soil Stockpile Angle Regression Tests

| Source of variance | Sum of squares | Degree of freedom | F | P |
|---|---|---|---|---|
| Model | 1.24 | 14 | 66.49 | <0.0001 |
| A-A | 0.0417 | 1 | 31.19 | 0.0001 |
| B-B | 0.2053 | 1 | 153.69 | <0.0001 |
| C-C | 0.198 | 1 | 148.2 | <0.0001 |
| D-D | 0.1014 | 1 | 75.89 | <0.0001 |
| AB | 0.0036 | 1 | 2.69 | 0.1266 |
| AC | 0.0961 | 1 | 71.93 | < 0.0001 |
| AD | 0.1122 | 1 | 83.99 | < 0.0001 |
| BC | 0.0812 | 1 | 60.79 | < 0.0001 |
| BD | 0.1089 | 1 | 81.51 | < 0.0001 |
| CD | 0.04 | 1 | 29.94 | 0.0001 |

| Source of variance | Sum of squares | Degree of freedom | F | P |
|---|---|---|---|---|
| A² | 0.0013 | 1 | 0.9487 | 0.3493 |
| B² | 0.1039 | 1 | 77.77 | <0.0001 |
| C² | 0.0005 | 1 | 0.3666 | 0.5561 |
| D² | 0.065 | 1 | 48.67 | <0.0001 |
| Residual | 0.016 | 12 | | |
| Lack of fit | 0.0156 | 10 | 6.67 | 0.1373 |
| Pure error | 0.0005 | 2 | | |
| Cor total | 1.26 | 26 | | |

Based on the ANOVA, the regression equation for saline soil accumulation angle Y1 was established, and after transformation, the regression model was as follows:

$$R_1 = 1.70 + 0.068A + 8.39B + 15.61C - 0.25D - 22.14A \times C + 0.39A \times D - 28.5B \times C + 0.55B \times D - 27.92B^2 + 0.006D^2 \quad (16)$$

From Table 5, it can be seen that the regression model p<0.001, indicating that the regression model for saline soil accumulation angle and soil hardsetting is extremely significant.

In order to explore the interaction effect of the four test factors on the response values, according to Table 5, the interaction of AC, AD, BC, and BD had a significant effect on the accumulation angle of saline soil with the response surface and contour distribution plots, as shown in Fig. 11.

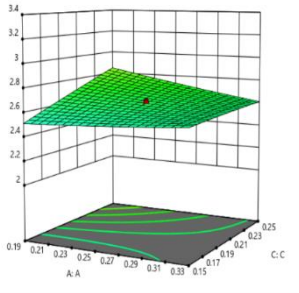

(a) Effect of AC on soil accumulation angle

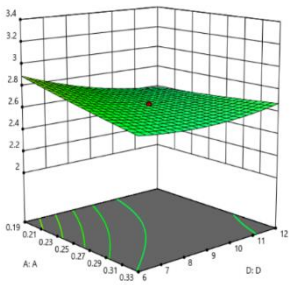

(b) Effect of AD on soil accumulation angle

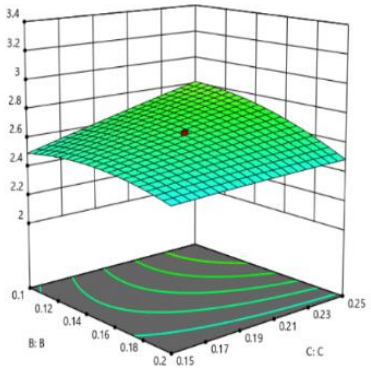

(c) Effect of BC on soil accumulation angle

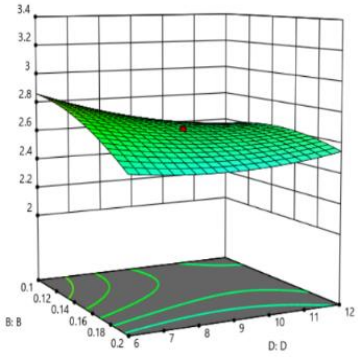

(d) Effect of BD on soil accumulation angle

**Fig. 11 – Saline soil accumulation angle interaction**

The curvature of the response surface shows that the interaction term affects the soil accumulation angle in the order of AD>BD>AC>BC, and the interaction term affects the soil hardsetting in the order of AC>AD>BD. It can be seen in Fig. 11(a) that the soil accumulation angle increases slowly with the collision recovery coefficient, and increases with the coefficient of kinetic friction, and the two interact with each other, and the soil accumulation angle almost does not change with the increase of the two simultaneously. It can be seen in Fig. 11(b) that the soil accumulation angle decreases with the increase of surface energy, but after interacting with the collision recovery coefficient, the soil accumulation angle appears to decrease and then increase as both increase. Fig. 11(c) shows that the soil accumulation angle tends to increase and then decrease as the static friction coefficient increases, and increases as the kinetic friction coefficient increases. They cancelled each other out and had a small effect on the soil accumulation angle. Fig. 11(d) shows that the soil accumulation angle increases with the decrease of static friction coefficient and JRK surface energy.

***Determination of optimal parameters***

In order to determine the optimal combination of contact parameters for saline soils, the minimum value of the difference between the soil accumulation angle and the soil hardsetting and the actual difference was taken as the target value, and the constraint equations were:

$$\begin{cases} Obj.\{minY_1 \\ s.t. \begin{cases} 0.12 \le A \le 0.40 \\ 0.05 \le B \le 0.30 \\ 0.10 \le C \le 0.45 \\ 3.50 \le D \le 14.5 \end{cases} \end{cases} \quad (17)$$

The results of obtaining the optimal solution are: coefficient of elastic recovery 0.262, coefficient of static friction 0.263, coefficient of kinetic friction 0.234, and JRK surface energy 10.084.

## CONCLUSIONS

In this study, the soil parameters in the test field were measured, and the soil density was 1622.5, the shear modulus was 3.76×107 Pa, the percentage distribution of saline soil particle size was mainly distributed in the interval of ＞2 mm sandy loam, and the type of saline soil can be obtained as chalky sandy clay according to the International Soil Classification Standard, the Poisson's ratio was 0.30. Due to the strong adhesion and elastic plasticity of saline soil, JKR was chosen as the contact model for saline soil and the contact parameters between saline soil particles (elastic recovery coefficient, static friction coefficient, dynamic friction coefficient, JRK surface energy) were taken as the test factors, and the soil stacking angle was taken as the test index for the saline soil contact parameter calibration. The test was conducted, and the quadratic regression equation was fitted, ANOVA and interaction effect analysis were performed to determine the optimal parameter combinations as: elasticity recovery coefficient 0.262, static friction coefficient 0.263, kinetic friction coefficient 0.234, and JRK surface energy 10.084 J/m$^2$.

This study has a certain role in advancing the research on constructing saline and alkaline soil models and analysing the interaction mechanism between saline and alkaline soils and the soil-entry components of agricultural machinery, especially in advancing the research on the mechanical properties of soil particles and changes in physical properties of soil touching the soil components of agricultural machinery operations in the process of excavation, trenching and other operations, which is crucial for the development of agricultural machinery and equipment applicable to saline and alkaline soils. However, the research in this paper mainly provides a method for constructing a structural soil discrete element particle contact model and parameter calibration, and the model parameters have complexity and variability under the conditions of soil characteristics and water content in different regions, which need to be reconstructed and calibrated according to soil type, particle size composition, water content and other factors.

## ACKNOWLEDGEMENT

The author was supported by the Shandong Province Technology Innovation Guidance Programme Project (YDZX2023005) and the Shandong Province Higher Educational Institutions Youth Creative Science, Technology Support Programme Project (2023KJ304) and the Youth Project of Natural Science Foundation of Shandong Province (ZR2022QE167).

## REFERENCES

[1] Abo-Elnor, M., Hamilton, R., Boyle, J.T. (2004). Simulation of soil-blade interaction for sandy soil using advanced 3D finite element analysis. *Soil and Tillage Research*, Vol. 75, pp 61-73, Cairo/Egypt.

[2] Aikins, K. A., Ucgul, M., Barr, J. B., Jensen, T. A., Antille, D. L., & Desbiolles, J. M. (2021). Determination of discrete element model parameters for a cohesive soil and validation through narrow point opener performance analysis. *Soil and Tillage Research*, Vol. 213, pp 105-123, Toowoomba/Australia.

[3] Chen, L., Mu, X., Peng, Z., (2021). Application of Discrete Element Method in Agricultural Engineering (离散元法在农业工程中的应用). *Agricultural Engineering*, Vol. 11, pp 29-34, Guangxi/China.

[4] Han, S., Qi, J., Kan, Z., Li, Y., Meng, H., (2021). Parameters Calibration of Discrete Element for Deep Application of Bulk Manure in Xinjiang Orchard (新疆果园深施散体厩肥离散元参数标定研究). *Trans. Chin. Soc. Agric. Mach*, Vol. 52, pp 101-108, Shihezi/China.

[5] Hao, Z., Zheng, E., Li, X., Yao, H., Wang, X., Qian, S., Li, W., Zhu, M., (2023). Performance analysis of the soil-contacting parts for no-tillage planters and optimization of blade structure (免耕播种机旋耕刀耕作性能分析与结构优化). *Transactions of the CSAE*, Vol. 39, pp 1-13, Nanjing/China.

[6] Li, J. W., Tong, J., Hu, B., Wang, H. B., Mao, C. Y., & Ma, Y. H. (2019). Calibration of parameters of interaction between clayey black soil with different moisture content and soil-engaging component in northeast China. *Transactions of the CSAE*, Vol. 35, pp 130-140, Shihezi/China.

[7] Luo, S., Yuan, Q., Gouda, Shaban., Yang, L., (2018). Parameters Calibration of Vermicomposting Nursery Substrate with Discrete Element Method Based on JKR Contact Model (基于 JKR 粘结模型的蚯蚓粪基质离散元法参数标定). *Trans. Chin. Soc. Agric. Mach*, Vol. 49, pp 343-350, Wuhan/China.

[8] Qiu, Y., Guo, Z., Jin, X., Zhang, P., Si, S., & Guo, F. (2022). Calibration and verification test of cinnamon soil simulation parameters based on discrete element method. *Agriculture*, Vol. 12, Luoyang/China.

[9] Song, Z., Li, H., Yan, Y., Tian, F., Li, Y., Li, F., (2010). Calibration Method of Contact Characteristic Parameters of Soil in Mulberry Field Based on Unequal-diameter Particles DEM Theory (桑园土壤非等径颗粒离散元仿真模型参数标定与试验). *Trans. Chin. Soc. Agric. Mach*, Vol. 53, pp 21-33, Taian/China.

[10] Tian, X., Cong, X., Qi, J., Guo, H., Li, M., Fan, X., (2021). Parameter Calibration of Discrete Element Model for Corn Straw-Soil Mixture in Black Soil Areas (黑土区玉米秸秆-土壤混料离散元模型参数标定). Trans. Chin. *Soc. Agric. Mach*, Vol. 52, pp 100-108, Changchun/China.

[11] Tong, J., Mohammad, M. A., Zhang, J., Ma, Y., Rong, B., Chen, D., & Menon, C. (2010). DEM numerical simulation of abrasive wear characteristics of a bioinspired ridged surface. *Journal of Bionic Engineering*, Vol. 7, pp 175-181, Changchun/China.

[12] Wang, X., Hu, H., Wang, Q., Li, H., He, J., Chen, W., (2017). Calibration Method of Soil Contact Characteristic Parameters Based on DEM Theory (基于离散元的土壤模型参数标定方法). Trans. Chin. *Soc. Agric. Mach*, Vol. 48, pp 78-85, Beijing/China.

[13] Wang, X., Zhang, S., Pan, H., Zheng, Z., Huang, Y., & Zhu, R. (2019). Effect of soil particle size on soil-subsoiler interactions using the discrete element method simulations. *Biosystems Engineering*, Vol. 182, pp 138-150, Yangling/China.

[14] Xing, J., Zhang, R., Wu P., Zhang, X., Dong, X., Chen, Y., Ru, S., (2020). Parameter calibration of discrete element simulation model for latosol particles in hot areas of Hainan Province (海南热区砖红壤颗粒离散元仿真模型参数标定). *Transactions of the CSAE*, Vol. 36, pp. 158-166, Hainan/China.

[15] Xu, Z., & Wang, J., (2005). Advances in Finite Element Analysis of Soil Cutting (有限元法分析土壤切削问题的研究进展). *Trans. Chin. Soc. Agric. Mach*, Vol. 36, pp. 134-137, China.

[16] Yu, J., Fu, H., Li, H., Shen, Y., (2005). Application of discrete element method to research and design of working parts of agricultural machines (离散元法及其在农业机械工作部件研究与设计中的应用). *Transactions of the CSAE*, Vol. 21, pp 1-6, Changchun/China.

[17] Zeng, Z., Ma, X., Cao, X., Li, Z., Wang, X., (2021). Critical Review of Applications of Discrete Element Method in Agricultural Engineering (离散元法在农业工程研究中的应用现状和展望). *Trans. Chin. Soc. Agric. Mach*, Vol. 52, pp 1-20, Guangzhou/China.

[18] Zhang, S., Zhao, H., Wang, X., Dong, J., Zhao, P., Yang, F., ... & Huang, Y. (2023). Discrete element modeling and shear properties of the maize stubble-soil complex. *Computers and Electronics in Agriculture*, Vol. 204, Yangling/China.